NANO LETTERS

Letter

pubs.acs.org/NanoLett

Nonlinear Correlation Spectroscopy (NLCS)

Matthias Geissbuehler,*[,†,∥] Luigi Bonacina,[‡] Vladislav Shcheslavskiy,[†,§] Noelia L. Bocchio,[†] Stefan Geissbuehler,[†] Marcel Leutenegger,[†] Iwan Märki,[†] Jean-Pierre Wolf,[‡] and Theo Lasser[†]

[†]Laboratoire d'Optique Biomédicale LOB, École Polytechnique Fédérale de Lausanne (EPFL), Switzerland

[‡]GAP-Biophotonics, Université de Genève, Switzerland

[§]Becker&Hickl GmbH, Berlin, Germany

S *Supporting Information*

ABSTRACT: We present a novel concept for optical spectroscopy called nonlinear correlation spectroscopy (NLCS). NLCS analyses coherent field fluctuations of the second and third harmonic light generated by diffusing nanoparticles. Particles based on noncentrosymmetric nonlinear materials such as $KNbO_3$ show a strong second as well as third harmonic response. The method and the theory are introduced and experimental NLCS results in fetal calf serum are presented showing the promising selectivity of this technique for measurement in complex biological environments.

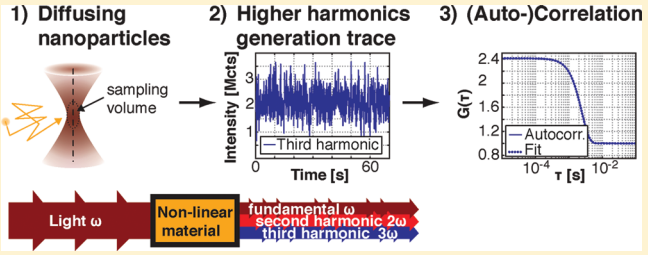

KEYWORDS: *Optical spectroscopy, fluorescence correlation spectroscopy (FCS), nonlinear correlation spectroscopy (NLCS), third-harmonic generation (THG), second-harmonic generation (SHG), nonlinear optics*

Many important questions in life science and medicine require a sensitivity at the single molecule level. This can be readily offered by fluorescence correlation spectroscopy (FCS).[1−3] FCS is a very popular and versatile tool that can be used to study a multitude of problems such as kinetics of enzymes,[4] RNA hybridization,[5] DNA conformational changes,[6,7] chemical reaction kinetics,[8] studies of phases and other membrane properties (in cellular and model membranes),[9−12] diffusion regimes in microchannels,[13] photophysics of fluorophores,[14] and many more.[8]

Current single-molecule methods are limited by their signal-to-noise ratio (SNR) at both short and long observation times. For fast processes, their SNR is determined by the lifetime and quantum yield of fluorescent labels and by the detection efficiency of the instrument. On the other hand, it is also difficult to measure slow processes with fluorescence methods because fluorophores hardly withstand long exposure times but tend to photobleach. Photobleaching typically restricts the total observation time to a few seconds, which complicates characterizing slow processes. In order to overcome these shortcomings, novel techniques based on nonlinear optics such as Raman correlation spectroscopy (RCS),[15] coherent anti-Stokes Raman scattering correlation spectroscopy (CARS-CS),[16,17] correlation spectroscopy of third-harmonic generation,[18] and sum-frequency scattering[19] have been developed. A novel approach named nonlinear correlation spectroscopy (NLCS) is presented here, which is also free from photobleaching and has the potential to become a valuable tool for spectroscopic measurements.

In classical optics, the induced polarization density depends linearly on the applied electric field $\mathbf{P}(t) = \mathbf{P}_{\mathrm{lin}} = \varepsilon_0\chi^{(1)}\mathbf{E}(t)$ where $\chi^{(1)}$ is the linear susceptibility and ε_0 is the free space permittivity. This holds for weak fields. For high intensities however, the relation becomes nonlinear leading to the generation of higher harmonic light.[20]

Techniques based on harmonic generation of light benefit from a coherent signal generation, which allows obtaining relatively strong and stable signals. The strengths of the harmonics scale with the nonlinear susceptibility and the qth power of the incident pumping field, which demands using short pulses of high intensity for good conversion efficiency. Because of the coherent interaction, the phases of all contributing fields should be matched over the lengths of the nonlinear material.

In bulk material, the third harmonic (TH) signal vanishes due to the destructive interference of the third harmonic signal generated in front of and behind of the focal plane. This cancelation is due to the Guoy phase shift across the focus.[20,21] On the other hand, nanoparticles (NP) with dimensions comparable to or smaller than the focal volume can generate strong higher harmonic signals. The phase mismatch between the harmonic signals and the incident wave is neglectable ($\ll\pi$) because NPs are small. Therefore any wavelength can be up-converted.[22] We use a chromium-activated forsterite laser (Cr:forsterite) emitting fs-pulsed light at a central wavelength

Received: January 6, 2012
Revised: February 22, 2012
Published: February 29, 2012

   dx.doi.org/10.1021/nl300070n | *Nano Lett.* 2012, 12, 1668−1672

of λ_0 = 1250 nm. Consequently both second harmonic (SH, at 625 nm) as well as TH (417 nm) light can be detected easily with standard optics. Such an approach is advantageous with respect to Ti:Sapphire laser-based systems, where the resulting TH appears in the deep-ultraviolet (DUV) at ≈260 nm and is therefore absorbed by most standard glasses employed in microscope objectives.

Because TH generation (THG) is a coherent process with directional emission, the collection efficiency can be improved and consequently a stronger signal is obtained. Unlike with CARS correlation spectroscopy, there is no background contribution in the TH signal because of the Gouy phase shift in NLCS. Further on, the setup needs only one unique laser line.

Figure 1A shows a schematic drawing of our setup. A detailed description can be found in the Supporting Information. We

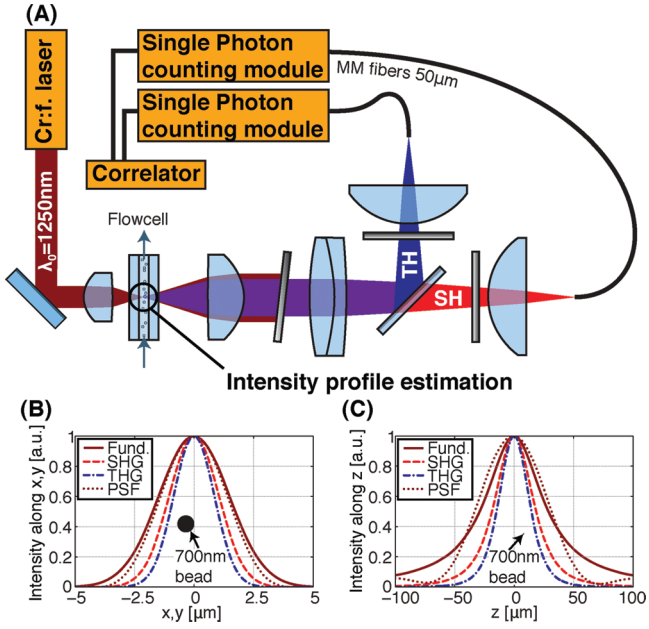

Figure 1. (A) Nonlinear correlation spectroscopy (NLCS) setup. The setup consists of a customized pulsed Cr:forsterite laser (peak power 150 kW), two aspheric lenses (excitation NA = 0.22), a flow cell driven by a peristaltic pump, a tube lens system, filters (heat absorber, dichroic beamsplitter, and respective emission filters for TH and SH), two multimode fibers, two fiber-coupled single photon counting modules, and a hardware correlator. (B,C) Intensity profile in *xy* and *z* as predicted by Zemax calculation (PSF) as well as by Gaussian beam approximation for the fundamental light intensity, as well as the SHG and THG profiles. The black dots are a representation of the PS nanoparticles for comparison with the size of the focal volume. See the Supporting Information for further details of the setup.

calculated the theoretical focal volume to be expected 300 μm inside the flow cell using an optical design software (Zemax). We approximated this profile by a focused Gaussian beam to reintroduce the optical phase and to calculate the SH and TH generation profiles.[20] As shown in Figure 1B,C, because of the different nonlinear power dependence the harmonic order influences the focal volume.

We have studied two different types of NPs: polystyrene spheres (PS d = 771 nm, Polysciences Inc.) and nonlinear $KNbO_3$ nanocrystals ($d \approx 120$ nm).[23]

Aggregation of PS was avoided by shaking and sonicating the PS suspensions prior to use. Before the measurements, the PS suspensions were circulated through the observation flow cell for several minutes for setting up well-defined PS concentrations.

When illuminating NPs with the Cr:forsterite laser, they can generate light of higher harmonic frequencies. Figure 2 shows

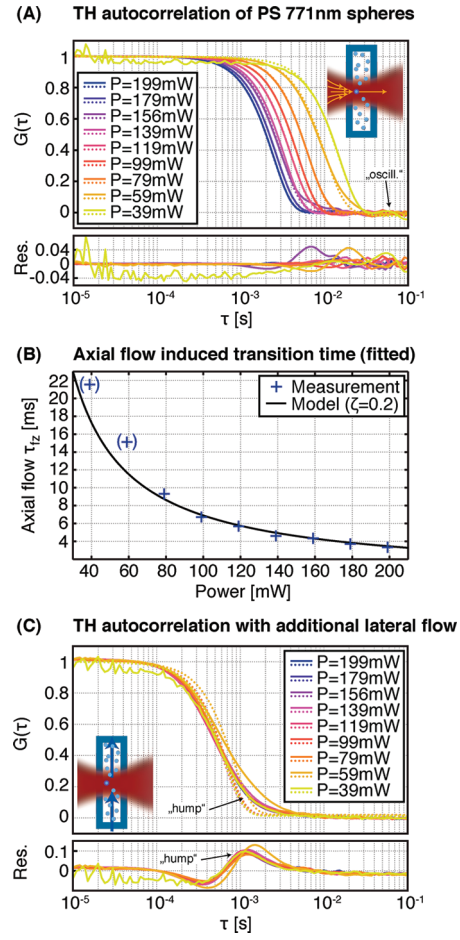

Figure 2. NLCS measurement of the radiation pressure effect as a function of the incident power for 700 nm PS spheres in water. (A) Measurement of the "free" diffusion (solid lines), fit by an NLCS model with flow (dotted lines) and fit residuals. (B) Plot of the fitted axial flow transition values with scaled model (ζ = 0.2). The values in parentheses have been excluded for the scaling-fit because of their low SNR. (C) When adding a small lateral flow (1 mL/min) by the peristaltic pump, the weak optical forces are no longer dominating and the radiation pressure dependency disappears. For all curve fits we fixed $\kappa_q = 0$ and $1/\tau_D = 0$ since the flow components appeared to be predominant. Each curve corresponds to an acquisition time of 60 s.

typical autocorrelations of the experimental intensity fluctuation of diffusing NPs. In order to improve the quality of the measurements, we have implemented an algorithm to suppress sample-related artifacts.[24] Furthermore, we found that the strong laser power exerts an optical force pushing the particles through the focus by radiation pressure as first shown by Ashkin.[25] Figure 2 shows the power dependency on the correlation curves. Starting from the radiation force along the optical axis[26−28] (also called scattering force) we calculate the maximum drag-force-limited velocity.[29] With our illumination NA of 0.22, the gradient force pulling the particles into the focus cannot compete with the much stronger scattering force. Therefore, we estimated that a 700 nm PS sphere would be

dx.doi.org/10.1021/nl300070n | *Nano Lett.* 2012, 12, 1668−1672

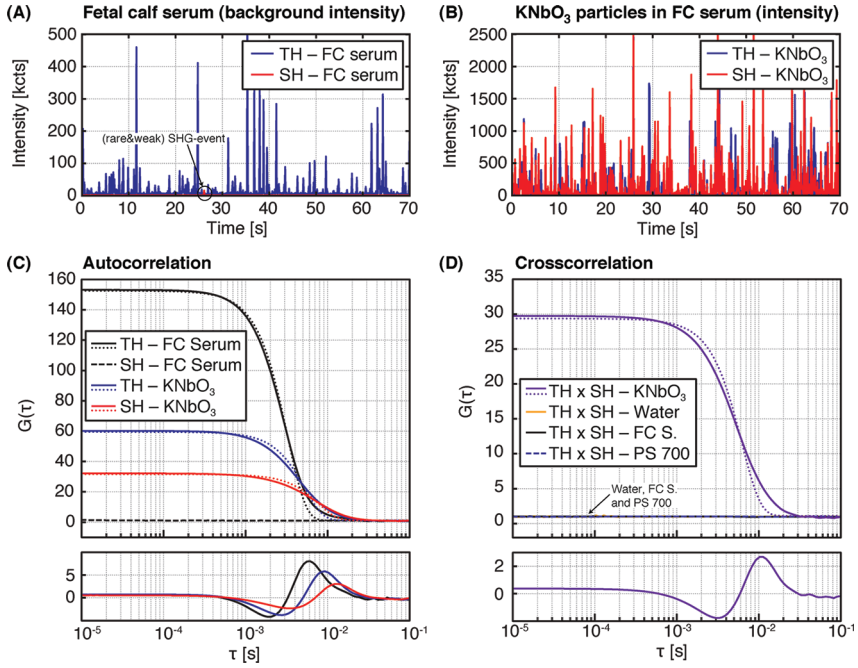

Figure 3. NLCS measurement in fetal calf (FC) serum. (A) Higher harmonic intensity of the FC serum (background). (B) Higher harmonic intensity of the $KNbO_3$ particles inside FC serum (TH background ≈ 1 kcts, SH background ≈ 0.4 kcts) (C) Autocorrelation curves for the SH and the TH intensity. The graph shows a comparison of the background (FC serum) to the $KNbO_3$ particles. (D) Crosscorrelation curves for KNbO3 particles, pure water, and PS spheres inside FC serum. The graph demonstrates the sensitivity to the $KNbO_3$ particles. For all fits, we fixed $\kappa_q = 0$ and $1/\tau_D = 0$ since the flow components appeared to be predominant. Each correlation curve corresponds to an acquisition time of 600 s. A mean illumination power of 240 mW was used.

accelerated to a velocity of $v_{max} \approx 100$ mm/s if illuminated with a laser power of 240 mW focused to a beam-waist of $\omega_0 = 2.7$ μm. This corresponds to a transition time through the focus of $\tau_{f_z} = z_0/v_z \approx 0.6$ ms for $z_0 = 54$ μm.

For the case of focusing into a suspension of freely diffusing particles, v_{max} can be used as an upper boundary for the expected mean velocity. However, since the particles are not only affected by radiation pressure, but also by Brownian motion and since the radiation force field is strongly dependent on the NP position, it is more reasonable to assume that the mean velocity is given by $v_{mean} = \zeta v_{max}$ where $\zeta < 1$. In Figure 2 B, we scaled the calculated model to fit the measured axial transition times and found $\zeta \approx 0.2$.

To fit the experimental curves, we developed a new model for (coherent) NLCS taking into account additional lateral flow. The model is related to a previously established model by Cheng et al. for CARS correlation spectroscopy.[17] We extend their model to higher harmonic generation from single (small) particles and include additional flow components.

The excitation amplitude can be approximated by a Gaussian focal volume taking into account the harmonic generation (i.e., $A_q(r)$ is the qth power of the fundamental Gaussian beam $A_1(r)$ to reflect the qth harmonic generation)

$$A_q(\mathbf{r}) \approx A_{q0} \exp\left(-\frac{x^2 + y^2}{\frac{\omega_0^2}{q}}\right) \exp\left(-\frac{z^2}{\frac{z_0^2}{q}}\right) \exp(-i\kappa_q z) \tag{1}$$

We include a linear phase term κ_q to incorporate a phase mismatch ($\Delta k = qk_1 - k_q$) as well as for an eventual approximation of the Gouy phase shift across the focal volume. Hence $\kappa_q z$ is a linear approximation of the axial phase of the excitation amplitude described by $\Theta(z) = q \arctan(z/z_g) - (qk_1 - k_q)z$, where the Gaussian beam approximation implies $z_g = b/2 = \pi\omega_0^2/\lambda_1$ with b as the confocal parameter.[20] In accordance to Boyd,[20] λ_1 represents the wavelength of the radiation in the medium ($\lambda_1 = 2\pi c/n\omega$).

With the approximation for the excitation amplitude given in eq 1, we derive an analytical expression for the normalized autocorrelation of the qth harmonic light intensity

$$G(\tau) = \frac{\langle I_q(t+\tau) I_q(t)\rangle - \langle I_q(t)\rangle^2}{\langle I_q(t)\rangle^2} = \frac{\langle \delta I_q(t+\tau)\delta I_q(t)\rangle}{\langle I_q(t)\rangle^2} \tag{2}$$

where $I_q(t)$ is the qth harmonic light intensity at time t, $\langle I_q(t)\rangle$ is the corresponding time-averaged intensity, and $\delta I_q(t) = I_q(t) - \langle I_q(t)\rangle$ is the intensity fluctuation at time t. We consider each particle as a point scatterer under Brownian motion. With these equations we derived an analytical model given in the Supporting Material along with some additional details of the derivation. As in FCS, this analytical model allows one to fit measured NLCS autocorrelation curves to yield model parameters such as the mean number of particles in the observation volume N, the mean diffusion time τ_D as well as the transition times through the focal volume induced by axial or lateral flow (τ_{fz} and τ_{fr} respectively).

Measuring in complex environments such as blood serum is a challenging task and requires high sensitivity in order to overcome background contributions. For instance, the autofluorescence typically prohibits sensitive fluorescence measurements in blood serum. With our instrument, we

dx.doi.org/10.1021/nl300070n | Nano Lett. 2012, 12, 1668–1672

performed NLCS in fetal calf serum (FC serum). We employed serum that had been inactivated by heating at 56 °C during 30 min and subsequently filtered with a pore size of 0.22 μm.

Although a SH field can be theoretically generated at any interface (including PS NPs surface) the yield of this process is quite low, and in our experimental conditions we were not able to detect any SH nonlinear signal. On the contrary, the use of noncentrosymmetric NPs can greatly enhance the nonlinear generation efficiency, because in this case the process originates from within the particle. To observe a SH signal, we used $KNbO_3$ NPs (orthorhombic crystal structure, point group *mm*2, dynamic light scattering (DLS) size before coating 120 nm) prepared by mechanical grinding, followed by selected centrifugation and deposition. The use of such noncentrosymmetric nanocrystals for SH sensing and imaging has been introduced recently and covers a wide family of nanomaterials.[22,30] This approach presents the advantages of high signal stability (i.e., no photobleaching), wavelength flexibility, and coherent SH and TH emission. A comprehensive survey covering the biological and biomedical potential of SH NPs has recently appeared.[31]

We first looked at the background signal of the fetal calf serum. Not surprisingly the serum contains structures emitting TH light (Figure 3A). Moreover, we could detect some rare and weak SH emission. This FC serum background showed a stable TH autocorrelation. After adding the $KNbO_3$ suspension, we observed strong higher harmonic generation both in the third and the second harmonic channel and obtained a stable and robust crosscorrelation between the two channels (Figure 3B–D).

Figure 3C shows the $KNbO_3$ autocorrelation curves in both channels. As expected, the SH channel showed a larger focal volume than the TH as confirmed both by the fitted number of particles inside the volume (N_{SH} = 0.035 and N_{TH} = 0.018) as well as by the fitted axial transit times ($\tau_{fz,SH}$ = 13 ms and $\tau_{fz,TH}$ = 9.1 ms).

For future work, it would be interesting to investigate the phase factor κ_q which has been kept constant (κ_q = 0) in the present analysis. Notably, in Figure 2A one can observe some oscillations for the low intensity curves (yellow), which indicate the validity of our flow model with the additional cosine terms (see Supporting Material). Furthermore the curves in Figure 2C have a significant "hump" at their tails which the fit did not account for. This might be another indication for a nonzero phase-factor. However it should also be noted that the fitting of the $KNbO_3$ particles' auto- and crosscorrelations are worse than for PS particles fit at medium and strong laser intensities. A possible explanation for this discrepancy could be the polydispersity of the $KNbO_3$ sample. In addition, our analytical correlation model assumes a laminar flow in the observation volume, which is only a first order approximation for the optical radiation pressure. An improved description should clearly take into account the position dependency of the optical forces.

In conclusion, we have introduced NLCS as a novel spectroscopic method with high sensitivity in complex environments for long-term observation of nonbleaching NPs with a high potential for more applications. These advantages enable sensing and tracking of single NPs as well as long-term imaging inside confined volumes, such as cells, where there is in general no quick renewal of labels. The nondestructive generation of SH and TH by nanoparticles overcomes the photobleaching limitations of fluorescence based methods. And multiharmonic detection combined with the crosscorrelation measurements provides unprecedented selectivity in physiological fluids or other complex environments. This approach can be further refined by the use of polarization resolved detection[32] or by resolving the emission anisotropy (e.g., forward vs backward emission).[33]

Furthermore, we have presented an analytical model to fit the coherent correlation curves. Our fit model accounts for lateral flow and for an axial flow induced by the radiation pressure. In addition NLCS provides a characterization of nanoparticles at the single particle level. NLCS is therefore an interesting tool for studying these labels, for example in aggregation tests or nonlinear-susceptibility studies.[34] Our NLCS implementation had the particularity that the strong illumination exerted notable radiation forces on the nanoparticles that pushed them through the focus. We performed initial experiments in a complex biological medium and showed measurements of particles in fetal calf serum that demonstrate the applicability and sensitivity of the method in this challenging environment.

■ ASSOCIATED CONTENT

Supporting Information

Additional details of the optical setup, particle preparation, theory for the optical forces estimation, development of the analytical NLCS fit model. This material is available free of charge via the Internet at http://pubs.acs.org.

■ AUTHOR INFORMATION

Corresponding Author

*E-mail: matthias.geissbuehler@epfl.ch.

Present Address

[‖]EPFL STI LOB - BM 5.138 - Station 17 - 1015 Lausanne, Switzerland.

Notes

The authors declare no competing financial interest.

■ ACKNOWLEDGMENTS

The authors thank Dr. D. Rytz, FEE - Forschungsinstitut für mineralische und metallische Werkstoffe Edelsteine/Edelmetalle GmbH, for providing $KNbO_3$ particles and Denis Ivanov for help with the Cr:forsterite laser setup. We acknowledge funding by the Swiss National Foundation (MCOCM project, 205321L_135353) and by the European FP7 project NAMDIATREAM (NMP-2009-4.0-3-246479).

■ REFERENCES

(1) Magde, D.; Elson, E.; Webb, W. *Phys. Rev. Lett.* **1972**, *29*, 705–708.
(2) Elson, E.; Magde, D. *Biopolymers* **1974**, *13*, 1–27.
(3) Rigler, R.; Mets, U.; Widengren, J.; Kask, P. *Eur. Biophys. J.* **1993**, *22*, 169–175.
(4) Hassler, K.; Rigler, P.; Blom, H.; Rigler, R.; Widengren, J.; Lasser, T. *Opt. Express* **2007**, *15*, 5366–5375.
(5) Schwille, P.; Bieschke, J.; Oehlenschläger, F. *Biophys. Chem.* **1997**, *66*, 211–228.
(6) Wennmalm, S.; Edman, L.; Rigler, R. *Proc. Natl. Acad. Sci. U.S.A.* **1997**, *94*, 10641–10646.
(7) Edman, L.; Mets, Ü.; Rigler, R. *Proc. Natl. Acad. Sci. U.S.A.* **1996**, *93*, 6710–6715.
(8) R Lakowicz, J. *Springer* **2006**, 954.
(9) Schwille, P.; Korlach, J.; Webb, W. *Cytometry* **1999**, *36*, 176–182.
(10) Korlach, J.; Schwille, P.; Webb, W.; Feigenson, G. *Proc. Natl. Acad. Sci. U.S.A.* **1999**, *96*, 8461–8466.

(11) Eggeling, C.; Ringemann, C.; Medda, R.; Schwarzmann, G.; Sandhoff, K.; Polyakova, S.; Belov, V. N.; Hein, B.; Von Middendorff, C.; Schönle, A.; Hell, S. W. *Nature* **2009**, *457*, 1159−1162.
(12) Strömqvist, J.; Chmyrov, A.; Johansson, S.; Andersson, A.; Mäler, L.; Widengren, J. *Biophys. J.* **2010**, *99*, 3821−3830.
(13) Durand, N.; Dellagiacoma, C.; Goetschmann, R.; Bertsch, A.; Märki, I.; Lasser, T.; Renaud, P. *Anal. Chem.* **2009**, *81*, 5407−5412.
(14) Widengren, J.; Mets, U.; Rigler, R. *J. Phys. Chem.* **1995**, *99*, 13368−13379.
(15) Schrof, W.; Klingler, J.; Rozouvan, S.; Horn, D. *Phys. Rev. E: Stat. Phys., Plasmas, Fluids, Relat. Interdiscip. Top.* **1998**, *57*, R2523−R2526.
(16) Hellerer, T.; Schiller, A.; Jung, G.; Zumbusch, A. *ChemPhysChem* **2002**, *3*, 630−633.
(17) Cheng, J.-X.; Potma, E. O.; Xie, S. *J. Phys. Chem. A* **2002**, *106*, 8561−8568.
(18) Jing, Y.; N'Gom, M.; Chang, Y.-C.; Agarwal, A.; Kotov, N.; Baker, J., Jr.; Norris, T. *Correlation spectroscopy of third-harmonic generation by single nanorods*. Proceedings of the 2009 Conference on Lasers and Electro-Optics and 2009 Conference on Quantum Electronics and Laser Science Conference, CLEO/QELS 2009, Baltimore, Maryland, May 31−June 5, 2009; CLEO: Washington, D.C., 2009.
(19) Dadap, J.; De Aguiar, H.; Roke, S. *J. Chem. Phys.* **2009**, *130*, 214710.
(20) Boyd, R. *Nonlinear optics*; Academic Press: New York, 2008; Chapters 1 and 2.
(21) Cheng, J.-X.; Xie, X. *J. Opt. Soc. Am. B* **2002**, *19*, 1604−1610.
(22) Extermann, J.; Bonacina, L.; Cuna, E.; Kasparian, C.; Mugnier, Y.; Feurer, T.; Wolf, J.-P. *Opt. Express* **2009**, *17*, 15342−15349.
(23) Nakayama, Y.; Pauzauskie, P. J.; Radenovic, A.; Onorato, R. M.; Saykally, R. J.; Liphardt, J.; Yang, P. *Nature* **2007**, *447*, 1098−U8.
(24) Ries, J.; Bayer, M.; Csúcs, G.; Dirkx, R.; Solimena, M.; Ewers, H.; Schwille, P. *Opt. Express* **2010**, *18*, 11073−11082.
(25) Ashkin, A. *Phys. Rev. Lett.* **1970**, *24*, 156−159.
(26) Ashkin, A. *Biophys. J.* **1992**, *61*, 569−582.
(27) Merenda, F. Micro-Optics for Multiple Laser Trapping in Microfluidics. Ph.D. thesis, Thesis, École Polytechnique Fédérale de Lausanne, Switzerland, 2008.
(28) Wright, W.; Sonek, G.; Berns, M. *Appl. Opt.* **1994**, *33*, 1735−1748.
(29) Additional details of this development can be found in the Supporting Information.
(30) Pantazis, P.; Maloney, J.; Wu, D.; Fraser, S. E. *Proc. Natl. Acad. Sci. U.S.A.* **2010**, *107*, 14535−14540.
(31) Staedler, D.; Magouroux, T.; Hadji, R.; Joulaud, C. *ACS Nano* **2012**, DOI: 10.1021/nn204990n.
(32) Bonacina, L.; Mugnier, Y.; Courvoisier, F.; Le Dantec, R.; Extermann, J.; Lambert, Y.; Boutou, V.; Galez, C.; Wolf, J.-P. *Appl. Phys. B* **2007**, *87*, 399−403.
(33) Dadap, J.; Shan, J.; Heinz, T. *J. Opt. Soc. Am. B* **2004**, *21*, 1328−1347.
(34) Shcheslavskiy, V.; Saltiel, S.; Faustov, A.; Petrov, G. I.; Yakovlev, V. *Opt. Lett.* **2006**, *31*, 1486−1488.